SIAM J. APPL. MATH.
Vol. 79, No. 3, pp. 986–1006

OPTIMAL CONTAINMENT OF EPIDEMICS OVER TEMPORAL ACTIVITY-DRIVEN NETWORKS*

MASAKI OGURA†, VICTOR M. PRECIADO‡, AND NAOKI MASUDA§

Abstract. In this paper, we study the dynamics of epidemic processes taking place in temporal and adaptive networks. Building on the activity-driven network model, we propose an adaptive model of epidemic processes, where the network topology dynamically changes due to both exogenous factors independent of the epidemic dynamics, as well as endogenous preventive measures adopted by individuals in response to the state of the infection. A direct analysis of the epidemic dynamics using Markov processes involves the eigenvalues of a transition probability matrix whose size grows exponentially with the number of nodes. To overcome this computational challenge, we derive an upper-bound on the decay ratio of the number of infected nodes in terms of the eigenvalues of a 2×2 matrix. Using this upper bound, we propose an efficient algorithm to tune the parameters describing the endogenous preventive measures in order to contain epidemics over time. We validate our theoretical results via numerical simulations.

Key words. temporal networks, adaptive networks, epidemics, stochastic processes, convex optimization

AMS subject classifications. 39A50, 60J10, 90C25, 91D10, 91D30

DOI. 10.1137/18M1172740

1. Introduction.

Accurate prediction and cost-effective containment of epidemics in human and animal populations are fundamental problems in mathematical epidemiology [9, 22, 37]. In order to achieve these goals, it is indispensable to develop effective mathematical models describing the spread of disease in complex contact networks [10, 12]. In this direction, we find a broad literature on modeling, analysis, and containment of epidemic processes in static contact networks. However, these works neglect an important factor, the temporality of the interactions [19, 48, 49], which arises either independently of or dependent on epidemic propagations. A framework for modeling temporal interactions in human and animal populations is temporal networks (i.e., time-varying networks), where individuals and interactions are modeled as nodes and edges, respectively, which can appear and disappear over time [17, 18, 32]. Under this framework, the effect of temporal interactions on epidemic propagations has been investigated numerically and theoretically [30, 31], resulting in a plethora of heuristic approaches [26, 40] and analytical methods [27, 34] for containing epidemic processes on temporal networks.

Adaptive networks refer to the case in which changes in nodes or edges occur in response to the state of the dynamics taking place on the network [12, 14, 32, 45].

*Received by the editors February 26, 2018; accepted for publication (in revised form) April 9, 2019; published electronically June 6, 2019.
http://www.siam.org/journals/siap/79-3/M117274.html
Funding: The work of the first author was supported by the Japan Society for the Promotion of Science under JSPS KAKENHI grant 18K13777. The work of the second author was supported by the U.S. National Science Foundation under grant CAREER-ECCS-1651433. The work of the third author was supported by the JST CREST grant JPMJCR1304 and the JST ERATO grant JPMJER1201, Japan.

†Division of Information Science, Nara Institute of Science and Technology, Ikoma, Nara (oguram@is.naist.jp).
‡Department of Electrical and Systems Engineering, University of Pennsylvania, Philadelphia, PA 19104 (preciado@seas.upenn.edu).
§Department of Engineering Mathematics, University of Bristol, Clifton, Bristol BS8 1UB (naoki.masuda@bristol.ac.uk).

A common temporality of agent-agent interaction in epidemic dynamics arises from social distancing behavior [2, 3, 4], which lets the structure of contact networks change over time as a result of adaptation to the state of the epidemics. Several models of such adaptive networks have been proposed. For example, Gross, D'Lima, and Blasius proposed a rewiring mechanism where a healthy node actively avoids being adjacent to infected nodes [13]. Extensions of this model are found in [12, 24, 29, 50, 54]. Guo et al. proposed an alternative model in which links connecting an infected node and a healthy node are deactivated [15]. As for the containment of epidemic processes on adaptive networks, various heuristic [6, 28] and analytical [33, 35] approaches have been proposed. However, in many studies, the effects of exogenous temporal factors and endogenous adaptive measures on epidemic processes have been separately examined, leaving unclear how their combination affects the dynamics of the spread.

In this paper, we study epidemic processes and containment strategies in a temporal network model where the effect of both exogenous factors and adaptive measures are simultaneously present. Our model is based on the activity-driven temporal network model [39]. In this model, a node is stochastically activated and connects to other nodes independently of the dynamics taking place in the network. In order to analyze the joint effect of exogenous factors and endogenous adaptations, we add a mechanism of social distancing to the standard activity-driven model. In other words, we allow an infected node to endogenously adapt to the state of the epidemics by (1) decreasing its activation probability and (2) refusing interactions with other activated nodes. On top of this temporal network, we adopt the standard susceptible-infected-susceptible (SIS) model of epidemic dynamics (see, e.g., [37]) and derive an analytical upper bound on the decay ratio of the number of infected nodes over time. Based on this result, we then propose an efficient strategy for tuning the social distancing rates in order to suppress the number of infected nodes.

Our work is related to [44], in which an infected individual is allowed to decrease its activation probability. However, in [44], the durations of temporal interactions are assumed to be sufficiently short compared with the time scale of the epidemic dynamics, leaving out the interesting case where the time scale of the network dynamics and that of the epidemic process are comparable. In addition, our results hold true for networks of any size, while the results in [44] require the networks to be sufficiently large.

This paper is organized as follows. In section 2, we introduce a model of epidemic processes on temporal and adaptive networks. In section 3, we derive an upper bound on the decay ratio of the infection size. Based on this bound, in section 4 we formulate and solve optimization problems for containing the spread of epidemics. The obtained theoretical results are numerically illustrated in section 5.

2. Problem setting. In this section, we first describe the activity-driven network proposed in [39]. We then introduce an adaptive SIS (A-SIS) model on activity-driven networks, which allows nodes to react to the state of the nodes (i.e., susceptible or infected) in their neighborhoods.

2.1. Activity-driven networks. Dynamics in real temporal networks often arise from time-varying nodal activities, such as messaging in the Twitter microblogging network, or the addition of publications in citation networks. The activity-driven network proposed in [39] incorporates time-varying nodal activities often observed in real-world networks.

Let the set of nodes in a network be given by $\mathcal{V} = \{v_1, \dots, v_n\}$. The activity-driven network model is defined as follows.

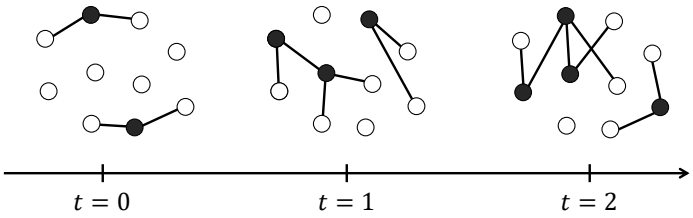

FIG. 1. *Schematic of an activity-driven network. We set* $n = 10$ *and* $m = 2$. *Filled circles represent active nodes. Open circles represent inactive nodes. The time is denoted by* t.

DEFINITION 2.1 (see [39]). *For each* $i = 1, \dots, n$, *let* a_i *be a positive constant less than or equal to* 1. *We call* a_i *the* activity rate *of node* v_i. *Let* m *be a positive integer less than or equal to* $n - 1$. *The* activity-driven network *is defined as an independent and identically distributed sequence of undirected graphs created by the following procedure (see Figure* 1 *for a schematic illustration):*

1. *At each time* $t = 0, 1, 2, \dots$, *each node* v_i *becomes "activated" with probability* a_i *independently of other nodes.*
2. *Each activated node, say,* v_i, *randomly and uniformly chooses* m *other nodes independently of other activated nodes. For each chosen node, say,* v_j, *an edge* $\{v_i, v_j\}$ *is created. These edges are discarded at time* $t + 1$ *(i.e., do not exist at time* $t + 1$*).*
3. *Steps* 2 *and* 3 *are repeated for each time* $t \geq 0$, *independently of past realizations.*

Remark 2.2. We do not allow multiple edges between a pair of nodes. In other words, even when a pair of activated nodes choose each other as their neighbors at a specific time, we assume that one and only one edge is spanned between those nodes.

The activity-driven network model has been increasingly used for modeling the structure and dynamics of temporal networks. The simplicity of the model allows us to analytically investigate the role of temporality and heterogeneity in temporal networks [20, 39, 51]. Several properties of activity-driven networks have been investigated, including structural properties [39, 47], steady-state properties of random walks [38, 43], and spreading dynamics [39, 44, 46]. However, the model does not assume that nodes react to the state of the epidemics and, therefore, is not relevant for discussing how social distancing affects the dynamics of the spread. In the next subsection, we extend the activity-driven network by incorporating social distancing behaviors of nodes.

2.2. Activity-driven A-SIS model. Building upon the activity-driven network described above, we consider the scenario where nodes change their neighborhoods in response to the state of the epidemics over the network [33]. Specifically, we propose the *activity-driven adaptive-SIS model* (*activity-driven A-SIS model*) as follows.

DEFINITION 2.3 (activity-driven A-SIS model). *For each* i, *let* $a_i, \chi_i, \pi_i \in (0, 1]$ *be constants. We call* a_i, χ_i, *and* π_i *the* activity rate, adaptation factor, *and* acceptance rate *of node* v_i, *respectively. Also, let* $m \leq n - 1$ *be a positive integer and* $\beta, \delta \in (0, 1]$ *be constants. The* activity-driven A-SIS model *is defined by the following procedures (see Figure* 2 *for an illustration):*

1. *At the initial time* $t = 0$, *each node is either* susceptible *or* infected.

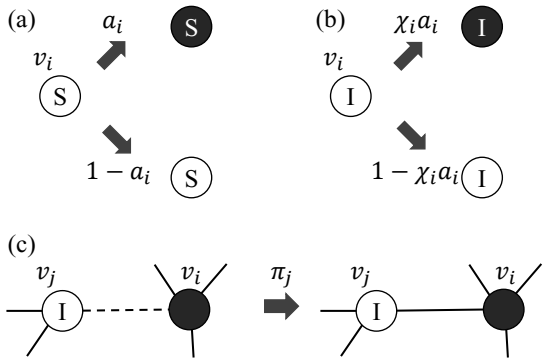

FIG. 2. *Adaptation of nodes in the activity-driven A-SIS model. Filled and empty circles represent active and inactive nodes, respectively.* (a) *A susceptible node is activated with probability* a_i. (b) *An infected node is activated with probability* $\chi_i a_i$. (c) *An infected node* (v_j) *accepts an edge spanned from an activated node with probability* π_j.

2. *At each time* $t = 0, 1, 2, \ldots$, *each node* v_i *randomly becomes activated independently of other nodes with the following probability:*

$$\Pr(\textit{node } v_i \textit{ becomes activated}) = \begin{cases} a_i & \textit{if } v_i \textit{ is susceptible,} \\ \chi_i a_i & \textit{if } v_i \textit{ is infected.} \end{cases} \tag{2.1}$$

3. *Each activated node, say,* v_i, *randomly and uniformly chooses* m *other nodes independently of other activated nodes. For each chosen node, say,* v_j, *an edge* $\{v_i, v_j\}$ *is created with the following probability:*

$$\Pr(\{v_i, v_j\} \textit{ is created}) = \begin{cases} 1 & \textit{if } v_j \textit{ is susceptible,} \\ \pi_j & \textit{if } v_j \textit{ is infected.} \end{cases} \tag{2.2}$$

   These edges are discarded at time $t+1$ *(i.e., do not exist at time* $t+1$*). As in Remark* 2.2*, we do not allow multiple edges between a pair of nodes.*
4. *The states of nodes are updated according to the SIS model. In other words, if a node* v_i *is infected, it transits to the susceptible state with probability* δ. *If* v_i *is susceptible, its infected neighbors infect node* v_i *with probability* β *independently of the other infected neighbors.*
5. *Steps* 2–4 *are repeated for each time* $t \geq 0$.

Steps 2 and 3 in Definition 2.3 model the social distancing behavior by infected nodes. In Step 2, an infected node decreases its activity rate to avoid infecting other nodes. Step 2 can also be regarded as modeling reduction of social activity by infected nodes due to sickness. In Step 3, an infected node, say, v_j, establishes a connection with an activated node only with probability π_j to avoid infecting other nodes (when $\pi_j < 1$). Once the connectivity of the network is determined, the nodes update their states. We adopt a synchronous update protocol, i.e., at each time t, the states of all nodes are updated simultaneously in Step 4.

3. Decay ratio. In order to quantify the persistence of epidemic infections in the activity-driven A-SIS model, in this section, we introduce the concept of decay ratio of the epidemics. A direct computation of the decay ratio requires computing the eigenvalues of a matrix whose size grows exponentially with the number of the

nodes. To overcome this difficulty, we present an upper bound on the decay ratio in terms of the eigenvalues of a 2×2 matrix.

3.1. Definition. For each time t and node v_i, define the random variable

$$x_i(t) = \begin{cases} 0 & \text{if } v_i \text{ is susceptible at time } t, \\ 1 & \text{if } v_i \text{ is infected at time } t. \end{cases} \tag{3.1}$$

Define the vector $p(t) = [p_1(t) \ \cdots \ p_n(t)]^\top$ of the infection probabilities by

$$p_i(t) = \Pr(v_i \text{ is infected at time } t). \tag{3.2}$$

Since $p_i(t) \leq 1$, there exist constants $C > 0$ and $\gamma \in [0, 1]$ such that

$$\|p(t)\| \leq C\gamma^t \tag{3.3}$$

for all $t \geq 0$, where $\|\cdot\|$ denotes a vector norm. In this paper, we measure the persistence of infection by the minimum ratio γ of decay of infection probabilities to the origin defined as follows.

DEFINITION 3.1 (see, e.g., [7, 52]). *We define the* decay ratio *of the activity-driven A-SIS model by*

(3.4)
$$\alpha = \inf\{\gamma\colon \textit{there exists } C > 0 \textit{ such that } (3.3) \textit{ holds true for all } t \geq 0 \textit{ and } x(0)\}.$$

The decay ratio is a basic quantity characterizing the asymptotic behavior of the spreading process. Besides quantifying the impact of contagious spreading processes over networks [11, 25], the decay ratio has been used for measuring the performance of strategies aiming to contain epidemic outbreaks [1, 16, 41, 53]. However, the decay ratio is difficult to compute for large networks for the following reason. The Markov process $\{x_1(t), \ldots, x_n(t)\}_{t \geq 0}$ has 2^n states. Let Q denote its $2^n \times 2^n$ transition probability matrix. Since the disease-free state is the unique absorbing state, it follows that

$$\alpha = \max\{|\lambda| : \lambda \text{ is an eigenvalue of } Q,\ |\lambda| < 1\}. \tag{3.5}$$

Because the size of the matrix Q grows exponentially fast with respect to the number of the nodes, a direct computation of the decay ratio is difficult for large networks.

Due to the difficulty in computing the decay ratio, it is common to rely on upper-bounds of the decay ratio [1, 16, 41, 53]. Upper-bounds quantify the worst-case impact of epidemic processes, as well as give a performance certificate for strategies aiming to contain epidemic outbreaks. In the next subsection, we derive an upper-bound on the decay ratio of the activity-driven A-SIS model.

3.2. An upper bound. We start with the following proposition, which allows us to upper-bound the infection probabilities using a linear dynamics.

PROPOSITION 3.2. *Let*

$$\bar{m} = m/(n-1) \tag{3.6}$$

and, for all i, define the constants

$$\phi_i = \bar{m}\chi_i a_i, \quad \psi_i = \bar{m}\pi_i a_i. \tag{3.7}$$

Then,

$$p_i(t+1) \le (1-\delta)p_i(t) + \beta \sum_{j=1}^{n} [1-(1-\psi_i)(1-\phi_j)]p_j(t) \tag{3.8}$$

for all nodes v_i and $t \ge 0$.

Proof. By the definition of the A-SIS dynamics on the activity-driven network, the nodal states $x_1, \ldots, x_n$ obey the following stochastic difference equation:

$$x_i(t+1) = x_i(t) - x_i(t)N_\delta^{(i)}(t) + (1-x_i(t)) \left[1 - \prod_{j \ne i} \left(1 - a_{ij}(t)x_j(t)N_\beta^{(ij)}(t) \right) \right], \tag{3.9}$$

where

$$a_{ij}(t) = \begin{cases} 1 & \text{if an edge } \{v_i, v_j\} \text{ exists at time } t, \\ 0 & \text{otherwise,} \end{cases} \tag{3.10}$$

and $\{N_\delta^{(i)}(t)\}_{t=0}^{\infty}$ and $\{N_\beta^{(ij)}(t)\}_{t=0}^{\infty}$ are independent and identically distributed random Bernoulli variables satisfying

$$N_\delta^{(i)}(t) = \begin{cases} 1 & \text{with probability } \delta, \\ 0 & \text{with probability } 1-\delta \end{cases} \tag{3.11}$$

and

$$N_\beta^{(ij)}(t) = \begin{cases} 1 & \text{with probability } \beta, \\ 0 & \text{with probability } 1-\beta. \end{cases} \tag{3.12}$$

On the right-hand side of (3.9), the second and third terms represent recovery and transmission events, respectively. (A similar equation for the case of static networks can be found in [7].)

The Weierstrass product inequality shows that

$$1 - \prod_{j \ne i} \left(1 - a_{ij}(t)x_j(t)N_\beta^{(ij)}(t) \right) \le \sum_{j \ne i} a_{ij}(t)x_j(t)N_\beta^{(ij)}(t). \tag{3.13}$$

Therefore, since the expectation of $x_i(t)$ equals $p_i(t)$, taking the expectation in (3.9) gives

$$p_i(t+1) \le p_i(t) - \delta p_i(t) + \beta \sum_{j \ne i} E[(1-x_i(t))a_{ij}(t)x_j(t)], \tag{3.14}$$

where $E[\cdot]$ denotes the expectation of a random variable.

Now, assume $i \ne j$. By the definition of the variables x_i and a_{ij}, it follows that

$$\begin{aligned} &E[(1-x_i(t))a_{ij}(t)x_j(t)] \\ &\quad = \Pr(v_i \text{ and } v_j \text{ are adjacent, } v_i \text{ is susceptible, and } v_j \text{ is infected at time } t) \\ &\quad = \Pr(v_i \text{ and } v_j \text{ are adjacent at time } t \mid \Xi_{i,j}^t) \Pr(\Xi_{i,j}^t), \end{aligned} \tag{3.15}$$

where the event $\Xi_{i,j}^t$ is defined by

$$\Xi_{i,j}^t = \text{“}v_i \text{ is susceptible and } v_j \text{ is infected at time } t\text{.”} \tag{3.16}$$

If we further define the event

$$\Gamma_{i\to j}^t = \text{“}v_i \text{ is activated and chooses } v_j \text{ as its neighbor at time } t\text{,”} \tag{3.17}$$

then we obtain

$$\begin{aligned} &\Pr(v_i \text{ and } v_j \text{ are adjacent at time } t \mid \Xi_{i,j}^t) \\ &\quad = \Pr(\Gamma_{i\to j}^t \mid \Xi_{i,j}^t) + \Pr(\Gamma_{j\to i}^t \mid \Xi_{i,j}^t) - \Pr(\Gamma_{i\to j}^t \mid \Xi_{i,j}^t)\Pr(\Gamma_{j\to i}^t \mid \Xi_{i,j}^t) \\ &\quad = 1 - \big[1 - \Pr(\Gamma_{i\to j}^t \mid \Xi_{i,j}^t)\big]\big[1 - \Pr(\Gamma_{j\to i}^t \mid \Xi_{i,j}^t)\big]. \end{aligned} \tag{3.18}$$

The event $\Gamma_{i\to j}^t$ occurs when and only when v_i is activated, chooses v_j as a potential neighbor, and actually connects to v_j (according to the probability given by (2.2)). Therefore, (3.7) implies

$$\Pr(\Gamma_{i\to j}^t | \Xi_{i,j}^t) = \psi_i. \tag{3.19}$$

Similarly, the event $\Gamma_{j\to i}^t$ occurs when and only when v_j is activated (with probability $\chi_j a_j$ if v_j is infected at time t) and chooses v_i as one of its m neighbors. Therefore, we have

$$\Pr(\Gamma_{j\to i}^t | \Xi_{i,j}^t) = \phi_j. \tag{3.20}$$

Hence, for $i \neq j$, the combination of (3.15) and (3.18)–(3.20) yields

$$\begin{aligned} E[(1 - x_i(t))a_{ij}(t)x_j(t)] &= [1 - (1 - \psi_i)(1 - \phi_j)]\Pr(\Xi_{i,j}^t) \\ &\le [1 - (1 - \psi_i)(1 - \phi_j)]p_j(t), \end{aligned} \tag{3.21}$$

where we have used the trivial inequality $\Pr(\Xi_{i,j}^t) \le p_j(t)$. Moreover, inequality (3.21) trivially holds true also when $i = j$. Inequalities (3.14) and (3.21) prove (3.8), as desired. ∎

Using Proposition 3.2, we obtain the following theorem that gives an explicit upper bound on the decay ratio of the activity-driven A-SIS model. For a vector $\xi \in \mathbb{R}^n$, introduce the notation

$$\langle \xi \rangle_a = \frac{1}{n}\sum_{i=1}^n a_i \xi_i, \quad \langle \xi \rangle_{a^2} = \frac{1}{n}\sum_{i=1}^n a_i^2 \xi_i. \tag{3.22}$$

THEOREM 3.3. *Define*

$$\alpha_{\mathrm{u}} = 1 - \delta + \kappa \bar{m} n \beta, \tag{3.23}$$

where

$$\kappa = \frac{\langle \chi \rangle_a + \langle \pi \rangle_a - \bar{m}\langle \chi\pi \rangle_{a^2} + \sqrt{\left(\langle \chi \rangle_a + \langle \pi \rangle_a - \bar{m}\langle \chi\pi \rangle_{a^2}\right)^2 + 4(\langle \chi\pi \rangle_{a^2} - \langle \chi \rangle_a \langle \pi \rangle_a)}}{2}. \tag{3.24}$$

Then, the decay ratio α satisfies

$$\alpha \le \alpha_{\mathrm{u}}. \tag{3.25}$$

Proof. Inequality (3.8) implies that there exists a nonnegative variable $\epsilon_i(t)$ such that

$$p_i(t+1) = (1-\delta)p_i(t) + \beta \sum_{j=1}^{n} \left(1 - (1-\psi_i)(1-\phi_j)\right) p_j(t) - \epsilon_i(t) \tag{3.26}$$

for all nodes v_i and $t \geq 0$. Let us define the vectors $\epsilon(t) = [\epsilon_1(t) \ \cdots \ \epsilon_n(t)]^\top$, $\phi = [\phi_1 \ \cdots \ \phi_n]^\top$, and $\psi = [\psi_1 \ \cdots \ \psi_n]^\top$. Equation (3.26) is rewritten as

$$p(t+1) = \mathcal{F}p(t) - \epsilon(t), \tag{3.27}$$

where

$$\mathcal{F} = (1-\delta)I + \beta \left[\mathbb{1}\mathbb{1}^\top - (\mathbb{1}-\psi)(\mathbb{1}-\phi)^\top\right], \tag{3.28}$$

$\mathbb{1}$ denotes the n-dimensional column vector whose entries are all one, and I denotes the $n \times n$ identity matrix. Since $\mathcal{F}$ and $\epsilon(t)$ are nonnegative entrywise, (3.27) leads to $p(t) = \mathcal{F}^t p(0) - \sum_{\ell=0}^{t} \mathcal{F}^{k-\ell}\epsilon(\ell) \leq \mathcal{F}^t p(0)$. This inequality shows

$$\alpha \leq \rho(\mathcal{F}), \tag{3.29}$$

where $\rho(\cdot)$ denotes the spectral radius of a matrix.

Now, we evaluate $\rho(\mathcal{F})$. Equation (3.28) is rewritten as $\mathcal{F} = (1-\delta)I + \beta\mathcal{A}$, where $\mathcal{A} = \mathbb{1}\mathbb{1}^\top - (\mathbb{1}-\psi)(\mathbb{1}-\phi)^\top$. Since $\mathcal{A}$ is nonnegative entrywise and $1-\delta \geq 0$, we obtain

$$\rho(\mathcal{F}) = 1 - \delta + \beta\rho(\mathcal{A}). \tag{3.30}$$

Furthermore, as we prove in Appendix A, it holds that

$$\rho(\mathcal{A}) = \rho(n\mathcal{B}), \tag{3.31}$$

where

$$\mathcal{B} = \begin{bmatrix} 1 & 1 - \langle\psi\rangle \\ -1 + \langle\phi\rangle & -1 + \langle\phi\rangle + \langle\psi\rangle - \langle\phi\psi\rangle \end{bmatrix}, \tag{3.32}$$

$$\langle\phi\rangle = \frac{1}{n}\sum_{i=1}^{n}\phi_i, \quad \langle\psi\rangle = \frac{1}{n}\sum_{i=1}^{n}\psi_i, \quad \langle\phi\psi\rangle = \frac{1}{n}\sum_{i=1}^{n}\phi_i\psi_i. \tag{3.33}$$

Matrix $\mathcal{B}$ has the characteristic equation

$$(1-\lambda)\langle\phi\psi\rangle = (\lambda - \langle\phi\rangle)(\lambda - \langle\psi\rangle) \tag{3.34}$$

having the roots

$$\lambda = \frac{\langle\phi\rangle + \langle\psi\rangle - \langle\phi\psi\rangle \pm \sqrt{\left(\langle\phi\rangle + \langle\psi\rangle - \langle\phi\psi\rangle\right)^2 + 4(\langle\phi\psi\rangle - \langle\phi\rangle\langle\psi\rangle)}}{2}. \tag{3.35}$$

The roots are real because

$$\left(\langle\phi\rangle + \langle\psi\rangle - \langle\phi\psi\rangle\right)^2 + 4(\langle\phi\psi\rangle - \langle\phi\rangle\langle\psi\rangle) \geq \left(\langle\psi\rangle - \langle\phi\rangle\right)^2 + \langle\phi\psi\rangle^2 > 0, \tag{3.36}$$

which follows from the trivial inequality $4\langle\phi\psi\rangle \geq 2\langle\phi\rangle\langle\phi\psi\rangle + 2\langle\psi\rangle\langle\phi\psi\rangle$. Therefore, by substituting (3.7) into (3.35), we obtain $\rho(\mathcal{B}) = \kappa\bar{m}$. This equation and (3.29)–(3.31) complete the proof of the theorem. ∎

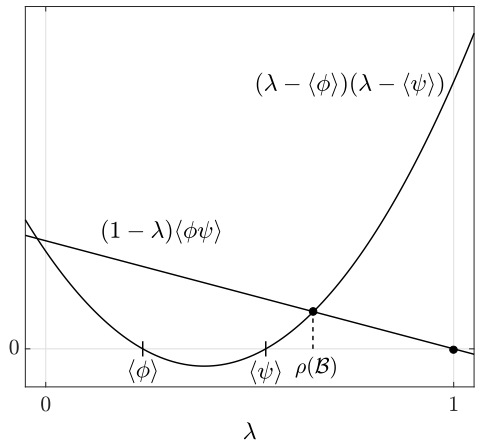

FIG. 3. *Characteristic equation* (3.34).

Remark 3.4. One of the main sources of the discrepancy between the actual decay ratio α and its upper bound α_{u} is in the upper-bounding approximation (3.13). In this approximation, the smaller the products $a_{ij}(t)x_j(t)N_\beta^{(ij)}(t)$ are, the tighter the inequality is. Therefore, we expect that, if β or m is smaller, the discrepancy $\alpha_{\mathrm{u}} - \alpha$ would be smaller. Numerical simulations carried out in section 5 confirm this prediction.

The following corollary suggests that an epidemic will become extinct more quickly when the adaptation factor and acceptance rate are less correlated in a weighted sense.

COROLLARY 3.5. *Let* (χ, π) *and* (χ', π') *be pairs of adaptation factors and acceptance rates of nodes, and denote the corresponding upper-bounds on the decay ratios by* α_{u} *and* α'_{u}*, respectively. If* $\langle\chi\rangle_a = \langle\chi'\rangle_a$*,* $\langle\pi\rangle_a = \langle\pi'\rangle_a$*, and* $\langle\chi\pi\rangle_{a^2} < \langle\chi'\pi'\rangle_{a^2}$*, then*

$$\alpha_{\mathrm{u}} < \alpha'_{\mathrm{u}}. \tag{3.37}$$

Proof. By the proof of Theorem 3.3, we have $\alpha_{\mathrm{u}} = 1-\delta+\rho(\mathcal{B})n\beta$. Figure 3 implies that $\rho(\mathcal{B})$ increases with $\langle\phi\psi\rangle$ when $\langle\phi\rangle$ and $\langle\psi\rangle$ are fixed. This proves the claim of the corollary because $\langle\chi\pi\rangle_{a^2} = \langle\phi\psi\rangle/\bar{m}^2$, $\langle\chi\rangle_a = \langle\phi\rangle/\bar{m}$, and $\langle\pi\rangle_a = \langle\psi\rangle/\bar{m}$. ∎

Corollary 3.5 has an intuitive implication. For the sake of discussion, let us temporarily assume that all nodes have the same activity rate. To maximize the correlation between χ and π while fixing the weighted sum of adaptation factors (i.e., $\langle\chi\rangle_a$) and that of acceptance rates (i.e., $\langle\pi\rangle_a$), we have to maximize the number of nodes that do not adopt any preventative behavior (i.e., $\chi_i = \pi_i = 1$). Therefore, when $\langle\chi\pi\rangle_{a^2}$ is large, only a limited fraction of the nodes implement preventative mechanisms, which is not effective in reducing the asymptotic decay ratio of the epidemic process in the entire temporal network.

As another corollary of Theorem 3.3, we also present an upper bound on the decay ratio when nodes do not adapt to the states of the nodes.

COROLLARY 3.6. *Assume* $\chi_i = \pi_i = 1$ *for all* i*. Let*

$$\kappa_0 = \frac{2\langle a\rangle - \bar{m}\langle a^2\rangle + \sqrt{4\langle a^2\rangle - 4\bar{m}\langle a\rangle\langle a^2\rangle + \bar{m}^2\langle a^2\rangle^2}}{2}. \tag{3.38}$$

Then, the decay ratio of the activity-driven SIS model is at most $1 - \delta + \kappa_0\bar{m}n\beta$.

Remark 3.7. If m is sufficiently small compared with n and, furthermore, n is sufficiently large (as implicitly assumed in [39]), the upper-bound in Corollary 3.6 reduces to $1-\delta+(\langle a\rangle+\sqrt{\langle a^2\rangle})m\beta$, which coincides with the result in [39].

4. Cost-optimal adaptations. In this section, we study the problem of eradicating an epidemic outbreak by distributing resources to nodes in the activity-driven network. Medications and vaccines are not necessarily available for emerging infectious diseases, such as the Ebola virus disease [8] and the Middle East respiratory syndrome [21]. In this situation, it is practically important to make sure that preventative behaviors are taken by members of the society to contain the spread of infectious diseases. Therefore, we consider the situation in which there is a budget that can be invested on strengthening the preventative behaviors of each node, instead of medications or vaccines. We show that the optimal budget allocation is found using geometric programs, which can be efficiently solved in polynomial time.

4.1. Problem statement. We consider an optimal resource allocation problem in which we can tune the adaptation factors and acceptance rates of nodes. Assume that, to set the adaptation factor of node v_i to χ_i, we need to pay a cost $f_i(\chi_i)$. Similarly we need to pay a cost $g_i(\pi_i)$ to set the acceptance rate of node v_i to π_i. The total cost for tuning the parameters to the values $\chi_1,\ldots,\chi_n$, $\pi_1,\ldots,\pi_n$ equals

$$C=\sum_{i=1}^{n}(f_i(\chi_i)+g_i(\pi_i)). \tag{4.1}$$

Throughout this section, we assume the following box constraints:

$$0<\underline{\chi}_i\le\chi_i\le\bar{\chi}_i,\quad 0<\underline{\pi}_i\le\pi_i\le\bar{\pi}_i. \tag{4.2}$$

In this paper, we consider the following two types of optimal resource allocation problems.

Problem 4.1 (cost-constrained optimal resource allocation). Given a total budget $\bar{C}$, find the adaptation rates and acceptance rates that minimize α_{u} while satisfying the budget constraint

$$C\le\bar{C}. \tag{4.3}$$

Problem 4.2 (performance-constrained optimal resource allocation). Given a largest tolerable decay ratio $\bar{\alpha}$, find the adaptation rates and acceptance rates that minimize the total cost C while satisfying the performance constraint

$$\alpha_{\mathrm{u}}\le\bar{\alpha}. \tag{4.4}$$

Remark 4.3. Although it would be desirable to formulate Problems 4.1 and 4.2 in terms of the true decay ratio, the true decay ratio is not computationally tractable for the reason described in subsection 3.1. Therefore, we use the upper-bound α_{u}, which is tight in the regime of low β or small m, as we shall verify in numerical simulations carried out in section 5.

4.2. Cost-constrained optimal resource allocation. In this subsection, we show that Problem 4.1 can be transformed to a geometric program [5], which can be efficiently solved. Before stating our main results, we give a brief review of geometric programs. Let $x_1,\ldots,x_n$ denote positive variables and define $x=(x_1,\ldots,x_n)$. We

say that a real function $q(x)$ is a *monomial* if there exist $c \geq 0$ and $a_1, \dots, a_n \in \mathbb{R}$ such that $q(x) = cx_1^{a_1} \cdots x_n^{a_n}$. Also, we say that a function $r(x)$ is a *posynomial* if it is a sum of monomials of x. (We point readers to [5] for more details.) Given a collection of posynomials $r_0(x)$, ..., $r_k(x)$ and monomials $q_1(x)$, ..., $q_\ell(x)$, the optimization problem

$$\begin{aligned} &\text{minimize} && r_0(x) \\ &\text{subject to} && r_i(x) \leq 1, \quad i = 1, \dots, k, \\ &&& q_j(x) = 1, \quad j = 1, \dots, \ell, \end{aligned} \tag{4.5}$$

is called a *geometric program*. A constraint of the form $r(x) \leq 1$ with $r(x)$ being a posynomial is called a *posynomial constraint*. Although geometric programs are not convex, they can be efficiently converted into equivalent convex optimization problems [5].

We assume that the cost functions f_i and g_i decrease with the adaptation factor χ_i and acceptance rate π_i, respectively. This assumption implies a natural situation in which it is more costly to suppress χ_i and π_i to a larger extent. We also expect diminishing returns with increasing investments [42]. For a fixed $\epsilon > 0$, let $\Delta f_i(\chi_i) = f_i(\chi_i - \epsilon) - f_i(\chi_i)$ denote the cost for improving the adaptation factor from χ_i to $\chi_i - \epsilon$. Then, diminishing returns imply that Δf_i decreases with χ_i, which implies the convexity of f_i. Therefore, we place the following assumption on the cost functions.

Assumption 4.4. For all $i \in \{1, \dots, n\}$, decompose f_i and g_i into the differences of their positive and negative parts as follows:

$$f_i = f_i^+ - f_i^-, \tag{4.6}$$

$$g_i = g_i^+ - g_i^-, \tag{4.7}$$

where $f_i^+ = \max(f, 0)$, $f_i^- = \max(-f, 0)$, $g_i^+ = \max(g, 0)$, and $g_i^- = \max(-g, 0)$. Then, f_i^+ and g_i^+ are posynomials, and f_i^- and g_i^- are constants.

Assumption 4.4 allows us to use any cost functions that are convex on the log-log scale because any function convex on the log-log scale can be approximated by a posynomial with an arbitrary accuracy [5, section 8]. We now state our first main result in this section, which allows us to efficiently solve Problem 4.1 via geometric programming.

THEOREM 4.5. *Let $\chi_i^\star$ and $\pi_i^\star$ be the solutions of the following optimization problem:*

$$\underset{\tilde{\lambda},\, \chi_i,\, \pi_i,\, \zeta,\, \eta > 0}{\text{minimize}} \quad 1/\tilde{\lambda} \tag{4.8a}$$

$$\text{subject to} \quad (4.2), \tag{4.8b}$$

$$\bar{m}^2 \tilde{\lambda} \langle \chi\pi \rangle_{a^2} \zeta\eta \leq 1, \tag{4.8c}$$

$$\zeta^{-1} + \tilde{\lambda} + \bar{m}\langle \chi \rangle_a \leq 1, \tag{4.8d}$$

$$\eta^{-1} + \tilde{\lambda} + \bar{m}\langle \pi \rangle_a \leq 1, \tag{4.8e}$$

$$\sum_{i=1}^n (f_i^+(\chi_i) + g_i^+(\pi_i)) \leq \bar{C} + \sum_{i=1}^n (f_i^- + g_i^-). \tag{4.8f}$$

Then, the adaptation factor $\chi_i = \chi_i^\star$ *and the acceptance rate* $\pi_i = \pi_i^\star$ *solve Problem* 4.1. *Moreover, under Assumption* 4.4, *the optimization problem* (4.8) *is a geometric program.*

To prove this theorem, we show an alternative characterization of the decay ratio in terms of inequalities.

LEMMA 4.6. *Let* $\lambda > 0$. *The upper bound* α_{u} *satisfies*

$$\alpha_{\mathrm{u}} \leq 1 - \delta + \lambda n \beta \tag{4.9}$$

if and only if

$$(1-\lambda)\langle \phi\psi \rangle \leq (\lambda - \langle \phi \rangle)(\lambda - \langle \psi \rangle), \tag{4.10}$$

$$\langle \phi \rangle < \lambda, \tag{4.11}$$

$$\langle \psi \rangle < \lambda. \tag{4.12}$$

Proof. By the proof of Theorem 3.3, inequality (4.9) holds true if and only if $\lambda \geq \rho(\mathcal{B})$. Figure 3 indicates that $\lambda \geq \rho(\mathcal{B})$ is equivalent to conditions (4.10)–(4.12). ∎

We can now prove Theorem 4.5.

Proof of Theorem 4.5. By Lemma 4.6, the solutions of Problem 4.1 are given by those of the following optimization problem:

$$\underset{\lambda,\, \chi_i,\, \pi_i > 0}{\text{minimize}} \quad 1 - \delta + \lambda n \beta \tag{4.13a}$$

$$\text{subject to} \quad \text{(4.2), (4.3), and (4.10)–(4.12).} \tag{4.13b}$$

Define the auxiliary variables $\zeta = 1/(\lambda - \langle \phi \rangle)$ and $\eta = 1/(\lambda - \langle \psi \rangle)$. Then, conditions (4.10)–(4.12) hold true if and only if $(1-\lambda)\langle \phi\psi \rangle \zeta\eta \leq 1$, $\zeta > 0$, and $\eta > 0$. Therefore, the optimization problem (4.13) is equivalent to the following optimization problem:

$$\underset{\lambda,\, \chi_i,\, \pi_i,\, \zeta,\, \eta > 0}{\text{minimize}} \quad \lambda \tag{4.14a}$$

$$\text{subject to} \quad \text{(4.2) and (4.3)}, \tag{4.14b}$$

$$(1-\lambda)\langle \phi\psi \rangle \zeta\eta \leq 1, \tag{4.14c}$$

$$\zeta^{-1} - \lambda + \langle \phi \rangle = 0, \tag{4.14d}$$

$$\eta^{-1} - \lambda + \langle \psi \rangle = 0, \tag{4.14e}$$

where we minimize λ instead of $1 - \delta + \lambda n \beta$. We claim that the optimal value of the objective function is equal to the one in the following optimization problem:

$$\underset{\lambda,\, \chi_i,\, \pi_i,\, \zeta,\, \eta > 0}{\text{minimize}} \quad \lambda \tag{4.15a}$$

$$\text{subject to} \quad \text{(4.2) and (4.3)}, \tag{4.15b}$$

$$(1-\lambda)\langle \phi\psi \rangle \zeta\eta \leq 1, \tag{4.15c}$$

$$\zeta^{-1} - \lambda + \langle \phi \rangle \leq 0, \tag{4.15d}$$

$$\eta^{-1} - \lambda + \langle \psi \rangle \leq 0. \tag{4.15e}$$

Let $\lambda_1^\star$ and $\lambda_2^\star$ be the optimal values of the objective functions in problems (4.14) and (4.15), respectively. We have $\lambda_1^\star \geq \lambda_2^\star$ because the constraints in problem (4.14)

are more strict than those in (4.15). Let us show $\lambda_1^\star \leq \lambda_2^\star$. Assume that the optimal value $\lambda_2^\star$ in problem (4.15) is attained by the parameters $(\lambda, \chi_i, \pi_i, \zeta, \eta) = (\lambda^\star, \chi_i^\star, \pi_i^\star, \zeta^\star, \eta^\star)$. Since the left-hand sides of constraints (4.15d) and (4.15e) decease with ζ and η, there exist nonnegative constants $\Delta\zeta$ and $\Delta\eta$ such that $\zeta = \zeta^\star - \Delta\zeta$ and $\eta = \eta^\star - \Delta\eta$ satisfy the equality constraints (4.14d) and (4.14e). Moreover, since the left-hand side of the constraint (4.15c) increases with ζ and η, the new set of parameters $(\lambda, \chi_i, \pi_i, \zeta, \eta) = (\lambda^\star, \chi_i^\star, \pi_i^\star, \zeta^\star - \Delta\zeta, \eta^\star - \Delta\eta)$ still satisfies (4.15c). Furthermore, these changes of parameters do not affect the feasibility of the box constraints (4.2) and the budget constraint (4.3) because the constraints are independent of the values of ζ and η. Therefore, we have shown the existence of parameters achieving $\lambda = \lambda_2^\star$ but still satisfying the constraints in the optimization problem (4.14). This shows $\lambda_1^\star \leq \lambda_2^\star$, as desired.

Now, by rewriting the optimization problem (4.15) in terms of the variables $\tilde{\lambda} = 1 - \lambda$ and substituting (3.7) in (4.15), we obtain the optimization problem (4.8). Notice that minimizing λ is equivalent to maximizing $1 - \tilde{\lambda}$, which is equivalent to minimizing $1/\tilde{\lambda}$.

Let us finally show that (4.8) is a geometric program. The objective function, $1/\tilde{\lambda}$, is a posynomial in $\tilde{\lambda}$. The constraints (4.2) and (4.8c)–(4.8e) are posynomial constraints. Finally, Assumption 4.4 guarantees that constraint (4.8f) is a posynomial constraint as well. This completes the proof of the theorem. ∎

4.3. Performance-constrained optimal resource allocation. In the same way as in the previous section, we can efficiently solve Problem 4.2 via geometric programming:

THEOREM 4.7. *Let $\chi_i^\star$ and $\pi_i^\star$ be the solution of the following optimization problem:*

$$\underset{\tilde{\lambda},\, \chi_i,\, \pi_i,\, \zeta,\, \eta > 0}{\text{minimize}} \quad \sum_{i=1}^{n} (f_i^+(\chi_i) + g_i^+(\pi_i)) \tag{4.16a}$$

$$\text{subject to} \quad \text{(4.2) and (4.8c)–(4.8e)}, \tag{4.16b}$$

$$\frac{\beta n + 1 - \delta - \bar{\alpha}}{\beta n} \tilde{\lambda}^{-1} \leq 1. \tag{4.16c}$$

Then, the adaptation factor $\chi_i = \chi_i^\star$ and the acceptance rate $\pi_i = \pi_i^\star$ solve Problem 4.2. Moreover, under Assumption 4.4, the optimization problem is a geometric program.

Proof. Constraint (4.16c) is equivalent to the performance constraint (4.4). The rest of the proof is almost the same as the proof of Theorem 4.5 and is omitted. ∎

5. Numerical simulations. In this section, we illustrate the theoretical results obtained in previous sections by numerical simulations.

5.1. Accuracy of the upper bound. We first illustrate the accuracy of the upper bound (3.23) on the decay rate. We use an activity-driven network with $n = 1000$ nodes and study the following two cases:

Case 1. Activity rates following a uniform distribution over $[0.001, 0.004]$.

Case 2. Activity rates following a probability distribution $F(a)$ that is proportional to $a^{-2.8}$ in the interval $[0.001, 1]$ and equal to zero elsewhere [39].

We assume that both the adaptation factors χ_i and acceptance rates π_i follow a uniform distribution over $[0, 1]$. For various values of β, δ, and m, we compute the decay ratio α based on numerical simulations of the model and its upper bound α_{u}. To

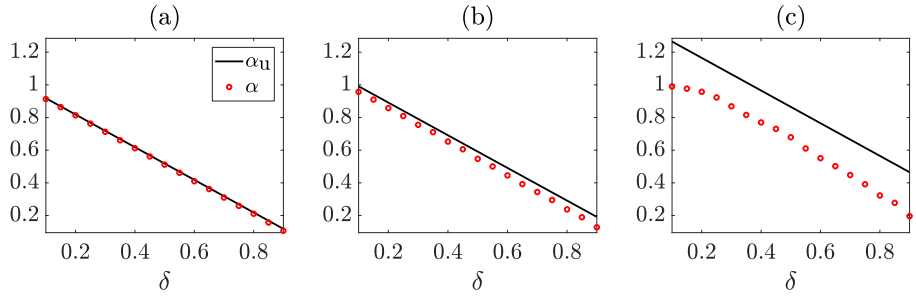

FIG. 4. *Comparison between the numerically obtained decay ratios α and their upper bounds α_u in Case 1 when $\beta = 0.7$.* (a) $m = 10$, (b) $m = 50$, *and* (c) $m = 200$.

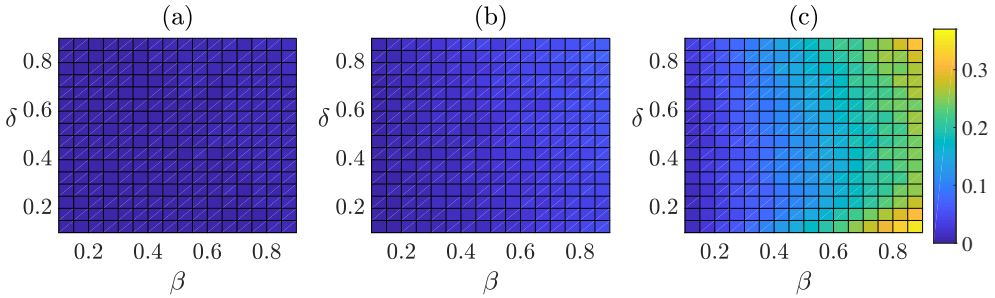

FIG. 5. *Discrepancy between the true decay ratios and their upper bounds in Case 1.* (a) $m = 10$, (b) $m = 50$, *and* (c) $m = 200$.

compute the decay ratio α, we use Monte Carlo simulations. For each triple (β, δ, m), we run 1000 simulations of the activity-driven A-SIS model with all nodes being infected at time $t = 0$. In each numerical simulation, we compute the probability vector $p(t)$ for each $t = 0, 1, 2, \ldots$ until the norm $\|p(t)\|$ falls below 0.1. We then estimate the decay ratio by $\alpha = \max_t t^{-1} \log\|p(t)\|$.

In Figure 4, we let $\beta = 0.7$ and compare the decay ratios and their upper bounds in Case 1 for various values of δ and m. We confirm that α_u bounds the numerically obtained decay ratios. The discrepancy $\alpha_u - \alpha$ increases with m. To further examine how the discrepancy depends on the parameters, we present the discrepancy for various values of β, δ, and m in Figure 5. Besides the aforementioned dependence of the discrepancy on m, we also see that the discrepancy tends to be large when β is large. We observe the same trend in the case of the power-law distribution of the activity rate (Case 2; shown in Figures 6 and 7).

5.2. Optimal resource distribution. We numerically illustrate our framework to solve the optimal resource allocation problems developed in section 4. We assume $\bar{\chi}_i = 1$ and $\bar{\pi}_i = 1$ in the box constraints (4.2). We use the following cost functions (similar to the ones in [41]):

$$f_i(\chi_i) = (1 - \underline{\chi}_i)\frac{\chi_i^{-p} - 1}{\underline{\chi}_i^{-p} - 1}, \quad g_i(\pi_i) = (1 - \underline{\pi}_i)\frac{\pi_i^{-q} - 1}{\underline{\pi}_i^{-q} - 1}. \tag{5.1}$$

These cost functions satisfy Assumption 4.4. Parameters $p, q > 0$ tune the shape of the cost functions as illustrated in Figure 8. Because the cost functions are normalized

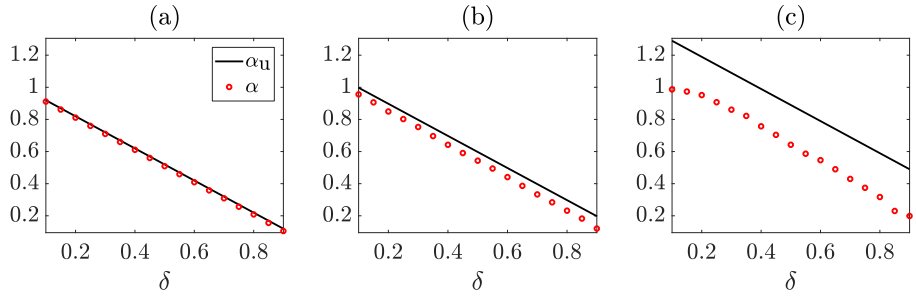

FIG. 6. *Comparison between the numerically obtained decay ratios* α *and their upper bounds* α_{u} *in Case* 2 *when* $\beta = 0.7$. (a) $m = 10$, (b) $m = 50$, *and* (c) $m = 200$.

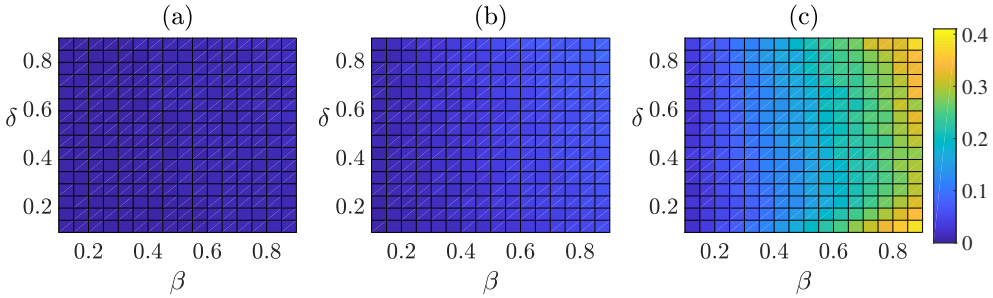

FIG. 7. *Discrepancy between the true decay ratios and their upper bounds in Case* 2. (a) $m = 10$, (b) $m = 50$, *and* (c) $m = 200$.

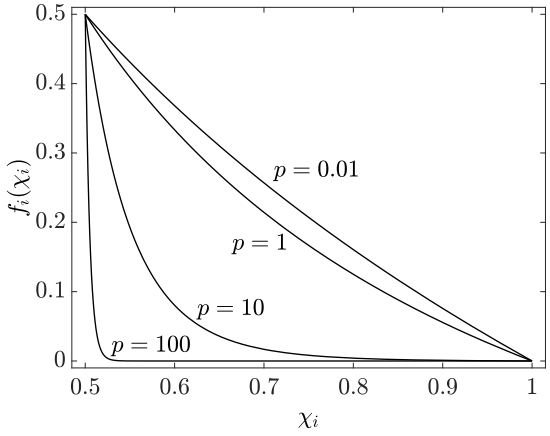

FIG. 8. *Cost function* $f_i(\chi_i)$ *for* $p = 0.01$, 1, 10, *and* 100 *when* $\underline{\chi}_i = 0.5$.

as $f_i(\underline{\chi}_i) = 1 - \underline{\chi}_i$, $f_i(\bar{\chi}_i) = f_i(1) = 0$, $g_i(\underline{\pi}_i) = 1 - \underline{\pi}_i$, and $g_i(\bar{\pi}_i) = g_i(1) = 0$, the maximum adaptation $(\chi_i, \pi_i) = (\underline{\chi}_i, \underline{\pi}_i)$ $(1 \le i \le n)$ in the network is achieved with the budget

$$C_{\max} = 2n - \sum_{i=1}^{n} (\underline{\chi}_i + \underline{\pi}_i). \tag{5.2}$$

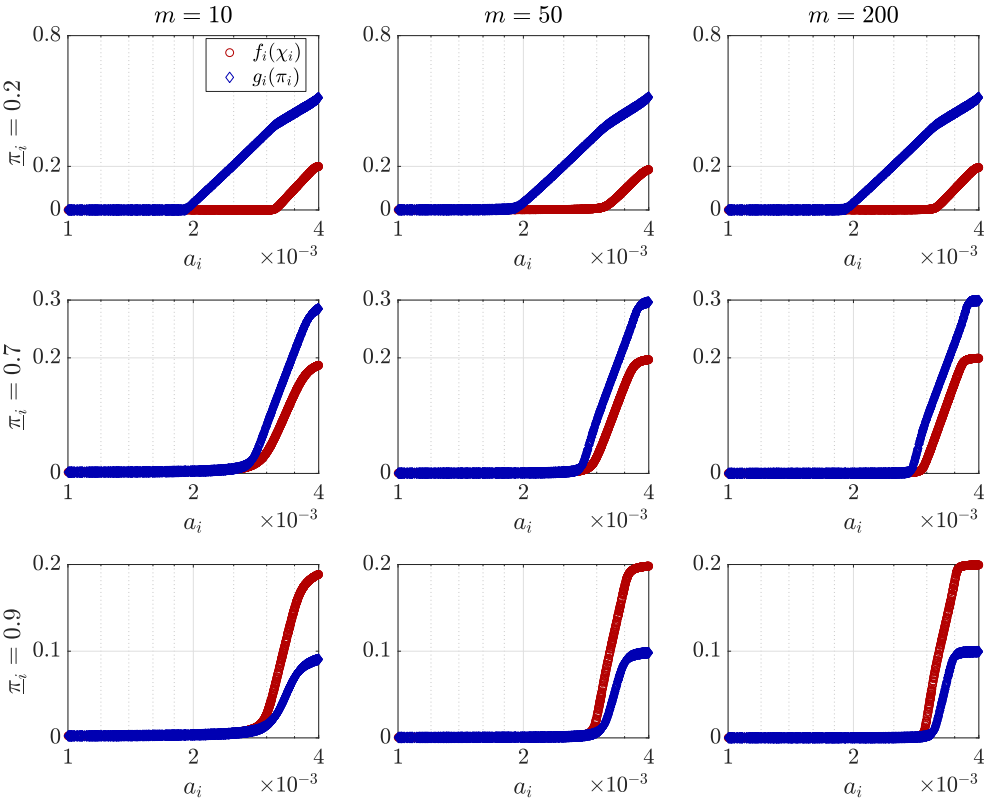

FIG. 9. *Optimal investments on adaptation factors (red circles) and acceptance rates (blue diamonds) in Case* 1. *Left column:* $m = 10$, *middle column:* $m = 50$, *right column:* $m = 200$. *Top row:* $\underline{\pi}_i = 0.2$, *middle row:* $\underline{\pi}_i = 0.7$, *bottom row:* $\underline{\pi}_i = 0.9$.

Let $\underline{\chi}_i = 0.8$. We let the value of $\underline{\pi}_i$ be either 0.2, 0.7, or 0.9 and use $p = q = 0.01$ for the cost functions (5.1). We use the fixed budget $\bar{C} = C_{\max}/4$. For each pair $(m, \underline{\pi}_i)$, we determinate the adaptation factors and acceptance rates for the cost-constrained optimal resource allocation problem (Problem 4.1) by solving the geometric program shown in Theorem 4.5.

The optimal investments on the adaptation factors and acceptance rates (i.e., $f_i(\chi_i)$ and $g_i(\pi_i)$) are shown in Figure 9 for Case 1. We see that the smaller the lower limit of the acceptance rate $\underline{\pi}_i$, the more we should invest on decreasing the acceptance rates. Also, the optimal solution disproportionately invests on the nodes having high activity rates. On the other hand, the optimal investments are almost independent on the value of m. We can observe similar trends from Case 2 shown in Figure 10.

Although the optimal investments on the adaptation factors and acceptance rates show a rather similar pattern, this similarity does not contradict the suggestion from Corollary 3.5 for the following reason: For the exponents $p = q = 0.01$, Figure 8 shows that the improvements in the adaptation factors and acceptance rates, i.e., $\Delta\chi_i = 1 - \chi_i$ and $\Delta\pi_i = 1 - \pi_i$, approximately satisfy $\Delta\chi_i \approx f(\chi_i)$ and $\Delta\pi_i \approx g(\pi_i)$. Hence, we can approximate the weighted correlation $\langle\chi\pi\rangle_{a^2}$ as

$$\langle\chi\pi\rangle_{a^2} \approx \langle f(\chi)g(\pi)\rangle_{a^2} - \langle f(\chi)\rangle_{a^2} - \langle g(\pi)\rangle_{a^2} + \langle 1\rangle_{a^2}. \tag{5.3}$$

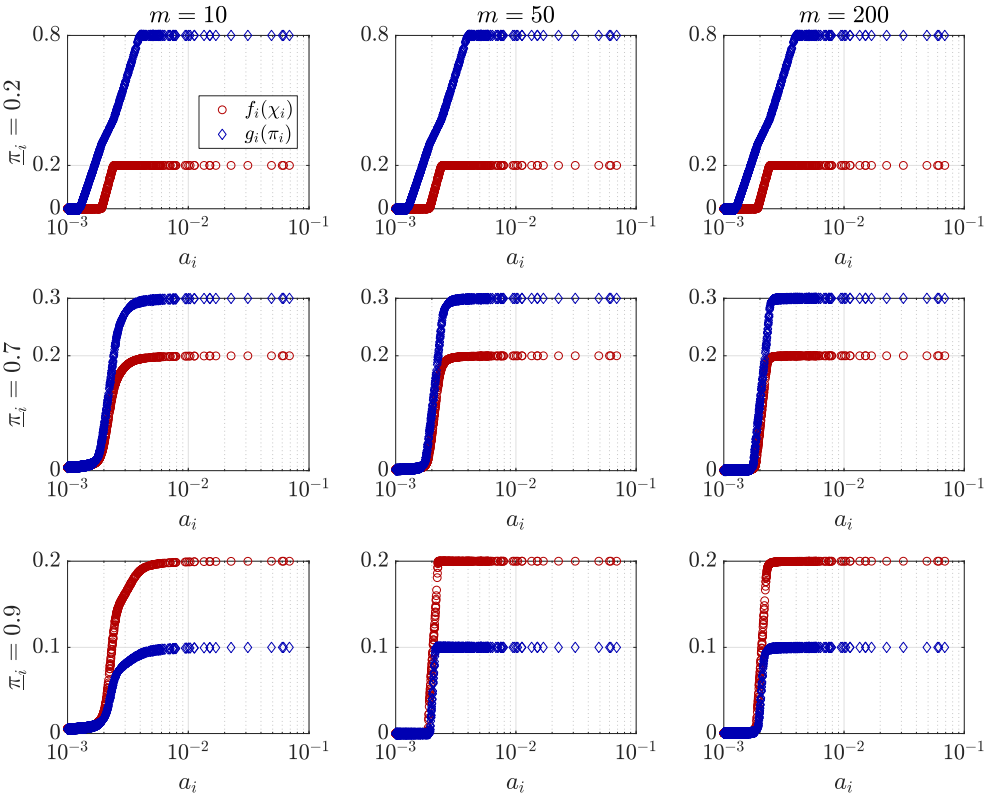

FIG. 10. *Optimal investments on adaptation factors (red circles) and acceptance rates (blue diamonds) in Case* 2. *Left column:* $m = 10$, *middle column:* $m = 50$, *right column:* $m = 200$. *Top row:* $\underline{\pi}_i = 0.2$, *middle row:* $\underline{\pi}_i = 0.7$, *bottom row:* $\underline{\pi}_i = 0.9$.

This relationship shows that, to achieve a smaller correlation $\langle \chi\pi \rangle_{a^2}$, we should either make the weighted investment-correlation $\langle f(\chi)g(\pi) \rangle_{a^2}$ smaller or make the weighted investments $\langle f(\chi) \rangle_{a^2}$ or $\langle g(\pi) \rangle_{a^2}$ larger. Therefore, simply minimizing the investment-correlation $\langle f(\chi)g(\pi) \rangle_{a^2}$ does not necessarily yield the best strategy.

In both Cases 1 and 2, when m is large, high-activity nodes receive large investments in not only the adaptation factor but also the acceptance rate. This result contradicts the intuition that the investments on acceptance rate become ineffective once a high-activity node becomes infected and turn into a major spreader of the infection. We, therefore, conjecture that the optimal investment primarily tries to prevent the high-activity nodes from becoming infected by investing in their acceptance rate.

6. Conclusion. In this paper, we have studied epidemic processes taking place in temporal and adaptive networks. Based on the activity-driven network model, we have proposed the activity-driven A-SIS model, where infected individuals adaptively decrease their activity and reduce connectivity with other nodes to prevent the spread of the infection. In order to avoid the computational complexity arising from the model, we have first derived a linear dynamics able to upper-bound the infection probabilities of the nodes. We have then derived an upper-bound on the decay ratio of the expected number of infected nodes in the network in terms of the eigenvalues of a 2×2 matrix. Then, we have shown that a small correlation between the two different

adaptation mechanisms is desirable for suppressing epidemic infection. Furthermore, we have proposed an efficient algorithm to optimally tune the adaptation rates in order to suppress the number of infected nodes in networks. We have illustrated our results by numerical simulations.

A possible direction for future research is to perform a more precise analysis by either improving the current upper bound or by deriving a lower bound on the decay ratio. One approach for improving the upper-bound is to tighten the inequality (3.13) by considering higher-order terms that are discarded by the Weierstrass product inequality. This change may allow us to obtain a tighter upper-bound on the decay ratio as done in [36] for the continuous-time SIS dynamics taking place in static networks. On the other hand, obtaining a lower bound is not necessarily a straightforward problem. For example, a converse of the Weierstrass product inequality [23] gives the following lower-bound on the expression on the left-hand side of (3.13):

$$1-\prod_{j\neq i}\left(1-a_{ij}(t)x_j(t)N_\beta^{(ij)}(t)\right)\geq\frac{\sum_{j\neq i}a_{ij}(t)x_j(t)N_\beta^{(ij)}(t)}{1+\sum_{j\neq i}a_{ij}(t)x_j(t)N_\beta^{(ij)}(t)}. \tag{6.1}$$

Unlike the upper-bound in (3.13), this lower-bound is not linear in the variables x_i. Therefore, obtaining a lower-bound on the decay ratio from (6.1) is not a trivial problem.

Another important problem is to directly minimize the number of infected nodes. By iteratively using (3.27), one can show that the number of infected nodes at time t, namely, $\mathbb{1}^\top p(t)=p_1(t)+\cdots+p_n(t)$, is upper-bounded by $\mathbb{1}^\top p(t)\leq\mathbb{1}^\top\mathcal{F}^t p(0)$. Therefore, we can implicitly minimize the number of infected nodes by minimizing the upper-bounding product $\mathbb{1}^\top\mathcal{F}^t p(0)$. However, since the matrix power $\mathcal{F}^t$ contains rather complex products of the vectors ψ and $\phi^\top$, a further investigation will be required to determine whether geometric programming can be used to minimize the upper-bounding product.

Appendix A. Proof of (3.31). The image of $\mathcal{A}$ is spanned by $\mathbb{1}$ and $\mathbb{1}-\psi$. All but two eigenvalues of $\mathcal{A}$ are zero. Therefore, an eigenvector of $\mathcal{A}$ corresponding to the spectral radius of $\mathcal{A}$ is a linear combination of vectors $\mathbb{1}$ and $\mathbb{1}-\psi$. Assume that $v=s_1\mathbb{1}+s_2(\mathbb{1}-\psi)$ is such an eigenvector of $\mathcal{A}$ with eigenvalue λ. By comparing the coefficients of the vectors $\mathbb{1}$ and $\mathbb{1}-\psi$ in the eigenvalue equation $\mathcal{A}v=\lambda v$, we obtain

$$s_1 n+s_2\left(n-\sum_{i=1}^n\psi_i\right)=\lambda s_1, \tag{A.1}$$

$$-s_1\left(n-\sum_{i=1}^n\phi_i\right)-s_2\left(n-\sum_{i=1}^n\psi_i-\sum_{i=1}^n\phi_i+\sum_{i=1}^n\psi_i\phi_i\right)=\lambda s_2. \tag{A.2}$$

We rewrite (A.1) and (A.2) as

$$n\mathcal{B}\begin{bmatrix}s_1\\ s_2\end{bmatrix}=\lambda\begin{bmatrix}s_1\\ s_2\end{bmatrix}, \tag{A.3}$$

where we have used the notation in (3.32) and (3.33). Therefore, λ is an eigenvalue of the matrix $n\mathcal{B}$, as desired.

REFERENCES

[1] J. Abad Torres, S. Roy, and Y. Wan, *Sparse resource allocation for linear network spread dynamics*, IEEE Trans. Automat. Control, 62 (2017), pp. 1714–1728, https://doi.org/10.1109/TAC.2016.2593895.

[2] J. E. Aledort, N. Lurie, J. Wasserman, and S. A. Bozzette, *Non-pharmaceutical public health interventions for pandemic influenza: An evaluation of the evidence base*, BMC Public Health, 7 (2007), 208, https://doi.org/10.1186/1471-2458-7-208.

[3] D. Bell, A. Nicoll, K. Fukuda, P. Horby, A. Monto, F. Hayden, C. Wylks, L. Sanders, and J. Van Tam, *Nonpharmaceutical interventions for pandemic influenza, national and community measures*, Emerging Infec. Dis., 12 (2006), pp. 88–94, https://doi.org/10.3201/eid1201.051371.

[4] M. C. J. Bootsma and N. M. Ferguson, *The effect of public health measures on the* 1918 *influenza pandemic in U.S. cities*, Proc. Natl. Acad. Sci. USA, 104 (2007), pp. 7588–7593, https://doi.org/10.1073/pnas.0611071104.

[5] S. Boyd, S.-J. Kim, L. Vandenberghe, and A. Hassibi, *A tutorial on geometric programming*, Optim. Eng., 8 (2007), pp. 67–127, https://doi.org/10.1007/s11081-007-9001-7.

[6] Y. Bu, S. Gregory, and H. L. Mills, *Efficient local behavioral-change strategies to reduce the spread of epidemics in networks*, Phys. Rev. E, 88 (2013), 042801, https://doi.org/10.1103/PhysRevE.88.042801.

[7] D. Chakrabarti, Y. Wang, C. Wang, J. Leskovec, and C. Faloutsos, *Epidemic thresholds in real networks*, ACM Trans. Inf. System Secur., 10 (2008).

[8] G. Chowell and H. Nishiura, *Transmission dynamics and control of Ebola virus disease (EVD): A review*, BMC Medicine, 12 (2014), 196, https://doi.org/10.1186/s12916-014-0196-0.

[9] O. Diekmann and J. A. P. Heesterbeek, *Mathematical Epidemiology of Infectious Diseases: Model Building, Analysis and Interpretation*, Wiley, New York, 2000.

[10] S. Funk, M. Salathé, and V. A. A. Jansen, *Modelling the influence of human behaviour on the spread of infectious diseases: A review*, J. Roy. Soc. Interface, 7 (2010), pp. 1247–1256, https://doi.org/10.1098/rsif.2010.0142.

[11] A. Ganesh, L. Massoulié, and D. Towsley, *The effect of network topology on the spread of epidemics*, in Proceedings of the 24th Annual Joint Conference of the IEEE Computer and Communications Societies, 2005, pp. 1455–1466.

[12] T. Gross and B. Blasius, *Adaptive coevolutionary networks: A review.*, J. Roy. Soc. Interface, 5 (2008), pp. 259–271, https://doi.org/10.1098/rsif.2007.1229.

[13] T. Gross, C. J. D. D'Lima, and B. Blasius, *Epidemic dynamics on an adaptive network*, Phys. Rev. Lett., 96 (2006), 208701, https://doi.org/10.1103/PhysRevLett.96.208701.

[14] T. Gross and H. Sayama, *Adaptive Networks*, Springer, Berlin, 2009.

[15] D. Guo, S. Trajanovski, R. van de Bovenkamp, H. Wang, and P. Van Mieghem, *Epidemic threshold and topological structure of susceptible-infectious-susceptible epidemics in adaptive networks*, Phys. Rev. E, 88 (2013), 042802, https://doi.org/10.1103/PhysRevE.88.042802.

[16] S. Han, V. M. Preciado, C. Nowzari, and G. J. Pappas, *Data-driven network resource allocation for controlling spreading processes*, IEEE Trans. Network Sci. Eng., 2 (2015), pp. 127–138, https://doi.org/10.1109/TNSE.2015.2500158.

[17] P. Holme, *Modern temporal network theory: A colloquium*, European Phys. J. B, 88 (2015); also available from https://arxiv.org/abs/1508.01303.

[18] P. Holme and J. Saramäki, *Temporal networks*, Phys. Rep., 519 (2012), pp. 97–125.

[19] L. Isella, J. Stehlé, A. Barrat, C. Cattuto, J. F. Pinton, and W. Van den Broeck, *What's in a crowd? Analysis of face-to-face behavioral networks*, J. Theoret. Biol., 271 (2011), pp. 166–180, https://doi.org/10.1016/j.jtbi.2010.11.033.

[20] M. Karsai, N. Perra, and A. Vespignani, *Time varying networks and the weakness of strong ties*, Sci. Rep., 4 (2014), 4001, https://doi.org/10.1038/srep04001.

[21] M. Ki, 2015 *MERS outbreak in Korea: Hospital-to-hospital transmission*, Epidemiol. Health, 37 (2015), e2015033, https://doi.org/10.4178/epih/e2015033.

[22] I. Z. Kiss, J. C. Miller, and P. L. Simon, *Mathematics of Epidemics on Networks*, Springer, Berlin, 2017.

[23] M. Klamkin and D. Newman, *Extensions of the Weierstrass product inequalities*, Math. Mag., 43 (1970), pp. 137–141, https://doi.org/10.2307/2688388.

[24] C. Lagorio, M. Dickison, F. Vazquez, L. A. Braunstein, P. A. Macri, M. V. Migueles, S. Havlin, and H. E. Stanley, *Quarantine-generated phase transition in epidemic spreading*, Phys. Rev. E, 83 (2011), 026102, https://doi.org/10.1103/PhysRevE.83.026102.

[25] A. Lajmanovich and J. A. Yorke, *A deterministic model for gonorrhea in a nonhomogeneous population*, Math. Biosci., 28 (1976), pp. 221–236, https://doi.org/10.1016/0025-5564(76)90125-5.

[26] S. Lee, L. E. C. Rocha, F. Liljeros, and P. Holme, *Exploiting temporal network structures of human interaction to effectively immunize populations*, PloS One, 7 (2012), e36439, https://doi.org/10.1371/journal.pone.0036439.

[27] S. Liu, N. Perra, M. Karsai, and A. Vespignani, *Controlling contagion processes in activity driven networks*, Phys. Rev. Lett., 112 (2014), 118702, https://doi.org/10.1103/PhysRevLett.112.118702.

[28] S. Maharaj and A. Kleczkowski, *Controlling epidemic spread by social distancing: Do it well or not at all*, BMC Public Health, 12 (2012), 679, https://doi.org/10.1186/1471-2458-12-679.

[29] V. Marceau, P. A. Noël, L. Hébert-Dufresne, A. Allard, and L. J. Dubé, *Adaptive networks: Coevolution of disease and topology*, Phys. Rev. E, 82 (2010), 036116, https://doi.org/10.1103/PhysRevE.82.036116.

[30] N. Masuda and P. Holme, *Predicting and controlling infectious disease epidemics using temporal networks*, F1000Prime Reports, 5 (2013), https://doi.org/10.12703/P5-6.

[31] N. Masuda and P. Holme, *Temporal Network Epidemiology*, Springer, Berlin, 2017, https://doi.org/10.1007/978-981-10-5287-3.

[32] N. Masuda and R. Lambiotte, *A Guide to Temporal Networks*, World Scientific, River Edge, NJ, 2016.

[33] M. Ogura and V. M. Preciado, *Epidemic processes over adaptive state-dependent networks*, Phys. Rev. E, 93 (2016), 062316, https://doi.org/10.1103/PhysRevE.93.062316.

[34] M. Ogura and V. M. Preciado, *Stability of spreading processes over time-varying large-scale networks*, IEEE Trans. Network Sci. Eng., 3 (2016), pp. 44–57, https://doi.org/10.1109/TNSE.2016.2516346.

[35] M. Ogura and V. M. Preciado, *Optimal Containment of Epidemics in Temporal and Adaptive Networks*, in Temporal Network Epidemiology, Springer, Berlin, 2017, pp. 241–266, https://doi.org/10.1007/978-981-10-5287-3.

[36] M. Ogura and V. M. Preciado, *Second-order moment-closure for tighter epidemic thresholds*, Systems Control Lett., 113 (2018), pp. 59–64, https://doi.org/10.1016/j.sysconle.2018.01.006.

[37] R. Pastor-Satorras, C. Castellano, P. Van Mieghem, and A. Vespignani, *Epidemic processes in complex networks*, Rev. Modern Phys., 87 (2015), pp. 925–979, arXiv:1408.2701.

[38] N. Perra, A. Baronchelli, D. Mocanu, B. Gonçalves, R. Pastor-Satorras, and A. Vespignani, *Random walks and search in time-varying networks*, Phys. Rev. Lett., 109 (2012), 238701, https://doi.org/10.1103/PhysRevLett.109.238701.

[39] N. Perra, B. Gonçalves, R. Pastor-Satorras, and A. Vespignani, *Activity driven modeling of time varying networks*, Sci. Rep., 2 (2012), https://doi.org/10.1038/srep00469.

[40] B. A. Prakash, H. Tong, N. Valler, M. Faloutsos, and C. Faloutsos, *Virus propagation on time-varying networks: Theory and immunization algorithms*, in Proceedings of the Joint European Conference on Machine Learning and Knowledge Discovery in Databases, 2010, pp. 99–114.

[41] V. M. Preciado, M. Zargham, C. Enyioha, A. Jadbabaie, and G. J. Pappas, *Optimal resource allocation for network protection against spreading processes*, IEEE Trans. Control Netw. Syst., 1 (2014), pp. 99–108, https://doi.org/10.1109/TCNS.2014.2310911.

[42] T. C. Reluga, *Game theory of social distancing in response to an epidemic*, PLoS Comput. Biol., 6 (2010), e1000793, https://doi.org/10.1371/journal.pcbi.1000793.

[43] B. Ribeiro, N. Perra, and A. Baronchelli, *Quantifying the effect of temporal resolution on time-varying networks*, Sci. Rep., 3 (2013), 3006, https://doi.org/10.1038/srep03006.

[44] A. Rizzo, M. Frasca, and M. Porfiri, *Effect of individual behavior on epidemic spreading in activity-driven networks*, Phys. Rev. E, 90 (2014), 042801, https://doi.org/10.1103/PhysRevE.90.042801.

[45] H. Sayama, I. Pestov, J. Schmidt, B. J. Bush, C. Wong, J. Yamanoi, and T. Gross, *Modeling complex systems with adaptive networks*, Comput. Math. Appl., 65 (2013), pp. 1645–1664, https://doi.org/10.1016/j.camwa.2012.12.005.

[46] L. Speidel, K. Klemm, V. M. Eguíluz, and N. Masuda, *Temporal interactions facilitate endemicity in the susceptible-infected-susceptible epidemic model*, New J. Phys., 18 (2016), 073013, https://doi.org/10.1088/1367-2630/18/7/073013.

[47] M. Starnini and R. Pastor-Satorras, *Topological properties of a time-integrated activity-driven network*, Phys. Rev. E, 87 (2013), 062807, https://doi.org/10.1103/PhysRevE.87.062807.

[48] J. Stehlé, N. Voirin, A. Barrat, C. Cattuto, L. Isella, J. F. Pinton, M. Quaggiotto, W. van den Broeck, C. Régis, B. Lina, and P. Vanhems, *High-resolution measurements of face-to-face contact patterns in a primary school*, PLoS ONE, 6 (2011), e23176, arXiv:1109.1015.

[49] L. Sun, K. W. Axhausen, D.-H. Lee, and X. Huang, *Understanding metropolitan patterns of daily encounters*, Proc. Natl. Acad. Sci. USA, 110 (2013), pp. 13774–13779, https://doi.org/10.1073/pnas.1306440110.

[50] I. Tunc and L. B. Shaw, *Effects of community structure on epidemic spread in an adaptive network*, Phys. Rev. E, 90 (2014), 022801, https://doi.org/10.1103/PhysRevE.90.022801.

[51] E. Ubaldi, N. Perra, M. Karsai, A. Vezzani, R. Burioni, and A. Vespignani, *Asymptotic theory of time-varying social networks with heterogeneous activity and tie allocation*, Sci. Rep., 6 (2016), 35724, https://doi.org/10.1038/srep35724.

[52] P. Van Mieghem, J. Omic, and R. Kooij, *Virus spread in networks*, IEEE/ACM Trans. Netw., 17 (2009), pp. 1–14, https://doi.org/10.1109/TNET.2008.925623.

[53] Y. Wan, S. Roy, and A. Saberi, *Designing spatially heterogeneous strategies for control of virus spread*, IET Syst. Biol., 2 (2008), pp. 184–201, https://doi.org/10.1049/iet-syb:20070040.

[54] D. H. Zanette and S. Risau-Gusmán, *Infection spreading in a population with evolving contacts*, J. Biol. Phys., 34 (2008), pp. 135–148, https://doi.org/10.1007/s10867-008-9060-9.